

---

# OASIS: Observation-Action Space Alignment via $SE(3)$ Trajectory Prediction for Robotic Manipulation

---

Xinzhe Chen\* Sihua Ren\* Liqi Huang Haowen Sun Mingyang Li  
Xingyu Chen Zeyang Liu Xuguang Lan†

National Key Laboratory of Human-Machine Hybrid Augmented Intelligence  
Institute of Artificial Intelligence and Robotics, Xi'an Jiaotong University

## Abstract

Recent vision-language-action (VLA) models and world action models (WAMs) advance robotic manipulation by enriching intermediate representations with auxiliary spatial features or future visual-state prediction. However, these representations largely remain within the observation space and do not share the rigid-body geometry of the action space, forcing the action decoder to implicitly recover this geometry. We propose OASIS, a visuomotor policy that aligns the intermediate representation with the action space via  $SE(3)$  end-effector trajectory prediction. OASIS couples a 3D-aware feature encoder that fuses vision-language and metric-depth features with an  $SE(3)$  trajectory predictor that produces a camera-frame end-effector trajectory. Conditioned on the predictor’s pose-supervised hidden states, the action decoder generates action chunks consistent with rigid-body motion. Across simulation and real-world experiments, OASIS outperforms VLA and WAM baselines in success rate and out-of-distribution generalization. Our project page is available at [https://npuhandsome.github.io/OASIS\\_web](https://npuhandsome.github.io/OASIS_web).

## 1 Introduction

Visuomotor policies for robotic manipulation use neural networks to map image observations, language instructions, and the robot state directly to executable 6-DoF actions and gripper commands [7, 11, 29, 39, 61, 67], with several representative families defining the current frontier. Vanilla Vision-Language-Action (VLA) models [3, 26, 27] build multimodal features from image observations and language instructions, typically via a pretrained Vision-Language Model (VLM), and feed these features directly into an action decoder [5, 22]. Feature-enhanced VLAs [19, 40, 41, 52] strengthen spatial understanding by injecting spatial features such as depth maps [28, 64], regions of interest [45], or 2D motion trajectories on the image plane [18, 23]. World Action Models (WAMs) [10, 13, 53] take a different route, learning a world model that predicts future images [17, 60] or latent visual features [33, 48, 51].

Rigid-body motions of a robot end-effector live in the Special Euclidean group  $SE(3)$ , yet a single image observation is consistent with many distinct 6-DoF actions under the same task instruction. Resolving this ambiguity requires an intermediate representation that constrains the target  $SE(3)$  pose. Despite their empirical strength, both VLA models and WAMs decode 6-DoF relative actions from intermediate representations that do not share the rigid-body geometry of the action space. Pretraining on large-scale robotic demonstrations or adding auxiliary spatial supervision can mitigate this ambiguity, but neither injects the geometric structure of  $SE(3)$  into the intermediate.

**Our key insight is that predicting an  $SE(3)$  end-effector trajectory aligns the intermediate representation with the action space, providing a geometric inductive bias rather than enriching**

---

\*Equal contribution.

†Corresponding author: [xgfan@mail.xjtu.edu.cn](mailto:xgfan@mail.xjtu.edu.cn)

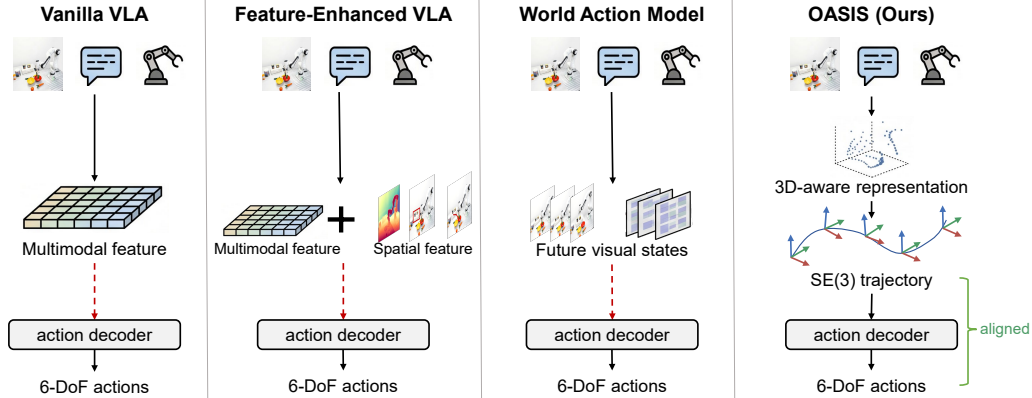


Figure 1: Comparison of existing visuomotor policies and OASIS. VLA models and WAMs construct intermediate representations that are not aligned with the action space. OASIS instead aligns the intermediate representation with the action space via  $SE(3)$  trajectory prediction.

**observation-space features with auxiliary spatial cues or predictive visual capacity.** We formalize this in Section 3.2. An intermediate representation is geometrically aligned when its pose-supervised component provides a readout of the target  $SE(3)$  state for action generation. Auxiliary supervision via future images, latent visual features, or 2D trajectories leaves pose recovery implicit in the decoder. In contrast,  $SE(3)$  end-effector trajectory prediction supervises the intermediate against the rigid-body geometry of the action space, giving the decoder a geometric inductive bias for action generation.

We instantiate this insight as **OASIS (Observation-Action Space Alignment via  $SE(3)$  Trajectory Prediction)**. OASIS couples three components trained end-to-end. A 3D-aware feature encoder fuses vision-language features with metric-depth features into a shared representation that supplies calibrated 3D spatial information. On this representation, an  $SE(3)$  trajectory predictor forecasts a sequence of camera-frame end-effector states. Predicting in the camera frame keeps the intermediate tethered to the observation stream and spares the predictor from learning the camera-to-world extrinsic. The predictor’s pose-supervised hidden states, which a linear head projects to this trajectory, condition the action decoder together with the current robot state, supplying the decoder with both the predicted geometry and the task-relevant context needed for execution. The decoder generates the action chunk while absorbing practical residuals such as the uncalibrated camera-to-world extrinsic and the gripper-timing offset. The prediction horizon matches the action-chunk length, and supervision is derived solely from standard expert demonstrations. OASIS therefore requires neither annotated spatial labels nor pretraining on large-scale robotic demonstrations.

Extensive experiments show that this alignment improves both simulation-benchmark and real-robot performance. On LIBERO [32], OASIS achieves a **97.6%** average success rate across the four suites. On CALVIN ABC→D [36], it attains a **4.57** average sequence length and an 83.3% success rate over five consecutive tasks. Ablations show that adding the  $SE(3)$  trajectory predictor to the 3D-aware feature encoder and decoder raises success from 89.5 to 95.2% on LIBERO-Long and from 91.6 to 99.0% on LIBERO-Spatial, the largest *additional* gain among ablated components. On a real-world setup across a Franka Research 3 and a Kinova Gen3 platform, OASIS reaches an 89.2% average success rate across multi-task, spatial-relationship, and long-horizon suites, outperforming  $\pi_{0.5}$  [5], RDT [35], Seer-Large [48], and ACT [63]. Moreover, under out-of-distribution (OOD) perturbations of the Goal task, covering unseen backgrounds, an altered camera viewpoint, and human interference, OASIS attains an average success rate of 90.8%. Our contributions are summarized as follows.

- We formulate an aligned-intermediate design principle for visuomotor policies, identifying  $SE(3)$  end-effector trajectory prediction as the mechanism that aligns the intermediate representation with the action space, providing a geometric inductive bias for action generation.
- We construct OASIS, a visuomotor policy coupling a 3D-aware feature encoder, an  $SE(3)$  trajectory predictor, and an action decoder, trained end-to-end on standard expert demonstrations without spatial annotations or large-scale robotic pretraining.

- Across simulation and real-world settings, OASIS consistently outperforms strong baselines in task success rate and on out-of-distribution perturbations, with ablations attributing the largest additional gain to the  $SE(3)$  trajectory predictor.

## 2 Related Work

**Vanilla Vision-Language-Action Models.** Vanilla VLA models map image observations and language instructions directly to 6-DoF actions through a multimodal encoder and a dedicated action decoder [8, 55]. Early work generates action chunks with autoregressive [47] or denoising action heads [37] such as ACT [63] and Diffusion Policy [12], followed by transformer-based variants [42, 43] including RDT-1B [35]. More recent methods leverage pretrained vision-language models [3, 27] for stronger semantic priors, including OpenVLA [22] on a Llama VLM [49] and  $\pi_0$  [5, 6] on a PaliGemma VLM [2] with flow matching [31]. The action decoder must recover depth and rotation from multimodal features alone, without a geometrically aligned intermediate.

**Feature-Enhanced VLA Models.** Feature-enhanced VLA models improve this image-to-action mapping by injecting auxiliary spatial features. One line lifts observations into 3D space [19, 24, 25, 56, 64]. SpatialVLA [40] encodes 3D position information via Ego3D position encoding, and QDepth-VLA [28] introduces quantized depth as auxiliary supervision. A complementary line provides task-relevant visual guidance [23, 52, 65]. ReconVLA [45] reconstructs gaze regions to focus attention on target objects, ThinkAct [18] predicts 2D end-effector trajectories, and UniVLA [9] derives task-centric action representations from videos. These features strengthen spatial reasoning and task understanding, yet the resulting intermediates do not share the rigid-body geometry of the action space, leaving the decoder to bridge them to actions. Structured-pose policies [14, 15, 21, 44] instead treat  $SE(3)$  poses as the final action representation, predicted from 3D inputs that require additional sensors or multi-view reconstruction. OASIS, in contrast, predicts an  $SE(3)$  trajectory from RGB images as the intermediate that conditions a learned action decoder.

**World Action Models.** World Action Models predict future images or latent visual features and decode actions from these predicted targets [53, 59]. SuSIE [4] synthesizes subgoal images via image editing as visual guidance. VPP [17] uses video diffusion models to predict future visual states as intermediate representations for action generation, and Seer [48] infers actions via inverse dynamics on predicted latent visual features. Related WAMs explore further couplings between visual prediction and action decoding [58, 60, 62, 66]. WorldVLA [10] formulates an autoregressive action-world model, and Unified-VLA [51] further unifies perception grounding, vision-supervised world modeling, and action generation within a single framework. Although these predictive intermediates make future visual-state structure explicit, they live on the image plane rather than sharing the rigid-body geometry of the action space, leaving the decoder to implicitly recover the rigid-body motion from these visual predictions.

## 3 Problem Formulation and Analysis

### 3.1 Problem Formulation

At time step  $t$ , a visuomotor policy  $\pi$  receives image observations  $\mathbf{o}_t$ , a language instruction  $l$ , and the current end-effector state  $\mathbf{e}_t = [\mathbf{p}_t, \boldsymbol{\theta}_t]^\top$ , with position  $\mathbf{p}_t \in \mathbb{R}^3$  and rotation parameterization  $\boldsymbol{\theta}_t$ . Equivalently,  $\mathbf{e}_t$  specifies a world-frame homogeneous transformation,

$$\mathbf{T}_t = \begin{bmatrix} \mathbf{R}(\boldsymbol{\theta}_t) & \mathbf{p}_t \\ \mathbf{0}^\top & 1 \end{bmatrix} \in SE(3), \quad (1)$$

where  $\mathbf{R}(\boldsymbol{\theta}_t) \in SO(3)$  is the corresponding rotation matrix.

Let  $\{\mathbf{T}_{t+h}\}_{h=1}^H$  denote a world-frame target pose sequence that successfully executes the manipulation task. The policy must produce an action chunk  $\mathbf{A}_t = \{(\mathbf{a}_{t+h-1}, g_{t+h-1})\}_{h=1}^H$  that drives the end-effector through this pose sequence, where  $\mathbf{a}_{t+h-1}$  is a 6-DoF relative end-effector action and  $g_{t+h-1}$  is the gripper command. For each horizon index  $h$ , the rigid-body component is recovered in closed form as

$$\mathbf{a}_{t+h-1} = \rho(\mathbf{T}_{t+h-1}^{-1} \mathbf{T}_{t+h}), \quad (2)$$

where  $\rho : SE(3) \rightarrow \mathbb{R}^6$  parameterizes a relative transformation as translation and rotation vectors (e.g., the axis-angle representation). Equation (2) converts any target pose sequence into executable 6-DoF relative actions. The gripper command is modeled separately because opening and closing the gripper is not a rigid-body motion in  $SE(3)$ .

### 3.2 Aligned Intermediate Representations of Visuomotor Policies

We model a visuomotor policy as a sequence of representation and action-decoding stages and adopt the following design principle. A horizon-indexed intermediate  $\mathbf{m}_t = \{\mathbf{m}_{t+h}\}_{h=1}^H$  is *geometrically aligned* with the action space if it provides an explicit pose readout  $r(\mathbf{m}_{t+h}) = \mathbf{g} \cdot \mathbf{T}_{t+h} \in SE(3)$  at each horizon step, where  $\mathbf{g} \in SE(3)$  is a fixed rigid transform that may be unknown. Given such a readout, the decoder applies the relative-action recovery of Eq. (2) while absorbing  $\mathbf{g}$ , prediction noise, contact dynamics, and gripper timing as residuals. We treat this as a design principle rather than a closed-form sufficiency theorem, since successful execution still depends on the residual control problem that the decoder must learn.

Vision-Language-Action (VLA) models, including feature-enhanced variants that inject auxiliary spatial features, encode the observation, instruction, and end-effector state into a latent multimodal feature and decode the action chunk directly,

$$\mathbf{z}_t = E_{\text{VLA}}(\mathbf{o}_t, l, \mathbf{e}_t), \quad \mathbf{A}_t = D_{\text{VLA}}(\mathbf{z}_t). \quad (3)$$

Because  $\mathbf{z}_t$  contains no explicit horizon-indexed pose readout,  $D_{\text{VLA}}$  must implicitly infer both the target poses  $\{\mathbf{T}_{t+h}\}_{h=1}^H$  and the parameterization  $\rho$  to realize Eq. (2). Pose recovery and action parameterization are therefore coupled inside a single learned action decoder.

WAMs insert a predictive intermediate representation before action decoding,

$$\mathbf{u}_t = F_{\text{WAM}}(\mathbf{o}_t, l, \mathbf{e}_t) \in \mathcal{P}^H, \quad \mathbf{A}_t = D_{\text{WAM}}(\mathbf{u}_t, \mathbf{e}_t), \quad (4)$$

where  $\mathcal{P}$  denotes an intermediate space such as future images or latent visual features. Although  $\mathbf{u}_t$  is horizon-indexed,  $\mathcal{P}$  does not share the rigid-body geometry of the action space. The decoder must therefore recover  $\mathbf{T}_{t+h}$  from  $\mathbf{u}_t$  before applying Eq. (2). WAMs thus expose temporal structure but leave the action-recovery step without geometric guidance.

OASIS instantiates this design principle by predicting a camera-frame  $SE(3)$  end-effector trajectory  $\{\mathbf{T}_{t+h}^c\}_{h=1}^H$ . This predicted trajectory satisfies the geometric-alignment property with  $\mathbf{g} = \mathbf{T}_{c \rightarrow w}^{-1}$ , the inverse of the camera-to-world extrinsic, since  $\mathbf{T}_{t+h}^c = \mathbf{T}_{c \rightarrow w}^{-1} \cdot \mathbf{T}_{t+h}$ . The decoder therefore receives explicit pose information for action generation up to this fixed rigid transform, and learns to absorb frame conversion, prediction noise, contact dynamics, and gripper timing as residuals.

## 4 Methodology

### 4.1 Overview of OASIS

OASIS instantiates the aligned-intermediate design principle from Section 3.2 with a three-stage policy architecture, illustrated in Figure 2. Since robotic manipulation acts in 3D physical space while image observations alone are 2D projections that lack metric depth, the 3D-aware feature encoder merges vision-language with metric-depth features into a 3D-aware representation  $\mathbf{h}_t^{3D}$ ,

$$\mathbf{h}_t^{3D} = E_{3D}(\mathbf{o}_t, l). \quad (5)$$

Conditioned on  $\mathbf{h}_t^{3D}$ , the trajectory predictor produces pose-supervised hidden states  $\mathbf{h}_{\text{traj}}$ , which a linear head projects to a horizon- $H$  camera-frame end-effector  $SE(3)$  trajectory  $\mathcal{T}_t^c$ . This trajectory prediction aligns the predictor’s intermediate representation with the action space,

$$\mathbf{h}_{\text{traj}} = P_{SE(3)}(\mathbf{h}_t^{3D}), \quad \mathcal{T}_t^c = \{\mathbf{T}_{t+h}^c \in SE(3)\}_{h=1}^H = \text{Linear}(\mathbf{h}_{\text{traj}}). \quad (6)$$

Predicting in the camera frame keeps the intermediate in the same frame as  $\mathbf{h}_t^{3D}$  and spares the predictor from learning the camera-to-world extrinsic. The action decoder, conditioned on these pose-supervised hidden states  $\mathbf{h}_{\text{traj}}$  and the current end-effector state  $\mathbf{e}_t$ , learns to approximate the relative-action recovery of Eq. (2) and emit gripper commands,

$$\mathbf{A}_t = D(\mathbf{h}_{\text{traj}}, \mathbf{e}_t). \quad (7)$$

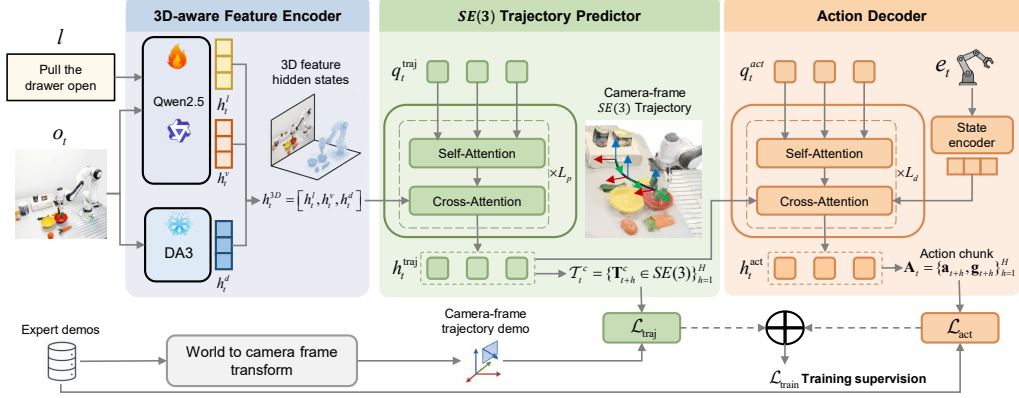


Figure 2: Architecture of OASIS. The 3D-aware feature encoder merges image, language, and metric-depth features into a 3D-aware representation. The  $SE(3)$  trajectory predictor aligns the intermediate representation with the action space via  $SE(3)$  trajectory prediction. The action decoder generates executable action chunks conditioned on this aligned intermediate representation.

## 4.2 3D-aware Feature Encoder

The encoder provides the predictor with a 3D-aware representation that preserves the language-conditioned visual information needed to forecast task-relevant target poses.

**Metric depth feature.** To supply the calibrated 3D structure that image observations lack, we use Depth Anything 3 [30], specifically the frozen DA3METRIC-LARGE model, which extracts multi-scale metric-depth features from  $\mathbf{o}_t$  and projects them into depth hidden states  $\mathbf{h}_t^d \in \mathbb{R}^{N_d \times D}$ .

**Vision-language feature.** For the vision-language features, we use a VLM with a Qwen2.5-0.5B backbone [1, 20] that jointly processes  $\mathbf{o}_t$  and  $l$ , producing visual hidden states  $\mathbf{h}_t^v \in \mathbb{R}^{N_v \times D}$  and language hidden states  $\mathbf{h}_t^l \in \mathbb{R}^{N_l \times D}$ . We concatenate the  $\mathbf{h}_t^l$ ,  $\mathbf{h}_t^v$ , and  $\mathbf{h}_t^d$  to form

$$\mathbf{h}_t^{3D} = [\mathbf{h}_t^l, \mathbf{h}_t^v, \mathbf{h}_t^d]. \quad (8)$$

## 4.3 $SE(3)$ Trajectory Predictor

The trajectory predictor aligns its intermediate representation with the action space by predicting  $\mathcal{T}_t^c$  from Eq. (6), where each  $\mathbf{T}_{t+h}^c \in SE(3)$  is the predicted end-effector state at horizon step  $h$ . A linear head projects the predictor’s hidden states  $\mathbf{h}_{\text{traj}}$  to this trajectory. These pose-supervised hidden states serve as the conditioning signal passed to the action decoder.

**Architecture.** The trajectory predictor initializes  $H$  learnable trajectory queries  $\mathbf{q}_{\text{traj}} \in \mathbb{R}^{H \times D}$ . Stacked transformer blocks process these queries with self-attention and Rotary Position Embeddings (RoPE) [46] for temporal coherence, while cross-attention conditions each query on  $\mathbf{h}_t^{3D}$ . The resulting trajectory hidden states  $\mathbf{h}_{\text{traj}} \in \mathbb{R}^{H \times D}$  are projected to per-step pose vectors

$$\boldsymbol{\tau}_t^c = \{\mathbf{e}_{t+h}^c = [\mathbf{p}_{t+h}^c, \boldsymbol{\theta}_{t+h}^c]^\top\}_{h=1}^H, \quad (9)$$

where  $\mathbf{p}_{t+h}^c \in \mathbb{R}^3$  is the position and  $\boldsymbol{\theta}_{t+h}^c \in \mathbb{R}^3$  is an axis-angle vector. Axis-angle is the canonical exponential-coordinate chart of  $SO(3)$ . Every prediction  $\boldsymbol{\theta}_{t+h}^c$  recovers a valid rotation matrix  $\mathbf{R}(\boldsymbol{\theta}_{t+h}^c) = \exp([\boldsymbol{\theta}_{t+h}^c]_\times) \in SO(3)$  in closed form via the Rodrigues rotation formula, so each pose vector induces a valid  $SE(3)$  element

$$\mathbf{T}_{t+h}^c = \begin{bmatrix} \mathbf{R}(\boldsymbol{\theta}_{t+h}^c) & \mathbf{p}_{t+h}^c \\ \mathbf{0}^\top & 1 \end{bmatrix} \in SE(3) \quad (10)$$

by construction, requiring no projection, Gram-Schmidt orthogonalization, or post-hoc correction. For the bounded range of camera-frame end-effector orientations encountered in tabletop manipulation we further have  $\|\boldsymbol{\theta}_{t+h}^c\| < \pi$ , keeping all predictions inside the canonical axis-angle chart of  $SO(3)$  and the network output on the  $SE(3)$  manifold throughout training and inference.

**Training objective.** For computational efficiency, we supervise the local pose parameterization with ground-truth pose vectors  $\hat{\tau}_t^c = \{\hat{\mathbf{e}}_{t+h}^c\}_{h=1}^H$  obtained by transforming world-frame demonstrations into the camera frame, and adopt the trajectory loss

$$\mathcal{L}_{\text{traj}} = \frac{1}{H} \sum_{h=1}^H \|\hat{\mathbf{e}}_{t+h}^c - \mathbf{e}_{t+h}^c\|_1. \quad (11)$$

We choose  $\ell_1$  because it is robust to teleoperation artifacts and yields precise pose modeling [63]. Empirically, this chart-space loss outperforms quaternion and Euler parameterizations under matched training (Table 3). In our setting, target and predicted absolute future orientations remain within the canonical axis-angle chart, away from the  $\|\theta_{t+h}^c\| = \pi$  singular set, so axis-angle coordinates are well-defined throughout training and inference.

#### 4.4 Action Decoder

The action decoder cross-attends to the predictor’s pose-supervised hidden states and the current end-effector state, approximating the relative-action recovery of Eq. (2) while absorbing frame conversion, prediction noise, contact dynamics, and gripper timing as residuals. We retain a learned decoder rather than a closed-form pose-to-action converter because these residuals exceed what explicit pose readouts can capture, as detailed in Appendix B.3.

**Architecture.** The action decoder initializes  $H$  learnable action queries  $\mathbf{q}_{\text{act}} \in \mathbb{R}^{H \times D}$ . These queries attend to two sources of context, namely the trajectory hidden states  $\mathbf{h}_{\text{traj}}$  from the predictor and a state embedding  $\mathbf{h}_{\text{state}} \in \mathbb{R}^{1 \times D}$  obtained by linearly projecting the current end-effector state  $\mathbf{e}_t$ . The two are concatenated into context hidden states  $\mathbf{h}_{\text{ctx}} = [\mathbf{h}_{\text{traj}}, \mathbf{h}_{\text{state}}] \in \mathbb{R}^{(H+1) \times D}$ . The decoder then outputs action chunks  $\mathbf{A}_t = \{(\mathbf{a}_{t+h-1}, g_{t+h-1})\}_{h=1}^H$ , where  $\mathbf{a}_{t+h-1} = [\Delta \mathbf{p}_{t+h-1}, \Delta \boldsymbol{\theta}_{t+h-1}]^\top$  is the 6-DoF relative action and  $g_{t+h-1}$  is the gripper command.

**Training objective.** The action loss supervises the output action chunk against expert demonstrations.

$$\mathcal{L}_{\text{act}} = \frac{1}{H} \sum_{h=1}^H \|[\hat{\mathbf{a}}_{t+h-1}, \hat{g}_{t+h-1}] - [\mathbf{a}_{t+h-1}, g_{t+h-1}]\|_1. \quad (12)$$

The total objective combines trajectory supervision with executable-action supervision,

$$\mathcal{L}_{\text{total}} = \lambda \mathcal{L}_{\text{traj}} + \mathcal{L}_{\text{act}}, \quad (13)$$

where  $\lambda$  balances the two losses and is set to 0.1.

## 5 Experiments

We evaluate OASIS in simulation and real-world settings, addressing four questions. First, whether OASIS surpasses VLA and WAM baselines on standard manipulation suites. Second, whether the metric-depth feature in the 3D-aware encoder is necessary. Third, how the supervision target on the predictor’s hidden states and its reference frame affect policy success. Fourth, whether OASIS’s lead transfers to real robots across multi-task suites and under out-of-distribution perturbations.

### 5.1 Implementation Details

The trajectory predictor and action decoder share a transformer architecture with four and two blocks respectively. The predictor outputs an eight-step  $SE(3)$  end-effector trajectory in the camera frame, and the decoder generates the corresponding action chunk conditioned on the trajectory hidden states. OASIS has 1.73B total parameters, of which 0.18B are trainable. We LoRA-tune [16] the Qwen2.5-0.5B VLM, train the predictor, decoder, and projection layers from scratch without large-scale robotic pretraining, and freeze DA3METRIC-LARGE [30]. Experiments use four NVIDIA A800 GPUs with batch size 64. Appendix A provides further details.

### 5.2 Simulation Experiments

**Simulation setup.** To answer the first question, we evaluate OASIS on two widely adopted simulation benchmarks, LIBERO [32] and CALVIN [36]. LIBERO has four task suites, namely Spatial, Object,

Table 1: Comparison of different methods on the LIBERO benchmark. The Pretrain column indicates whether the policy is pre-trained on large-scale robotic datasets, and the Intermediate column lists the representation each method feeds into the action decoder. The highest success rate in each suite is shown in bold.

Method	Intermediate	Pretrain	Spatial	Object	Goal	Long	Average
SpatialVLA [40]	spatial features	✓	88.2	89.9	78.6	55.5	78.1
WorldVLA [10]	future visual states	×	85.6	89.0	82.6	59.0	79.1
ThinkAct [18]	2D-supervised features	✓	88.3	91.4	87.1	70.9	84.4
$\pi_0$ [6]	multimodal features	✓	96.8	<b>98.8</b>	95.8	85.2	94.1
QDepth-VLA [28]	spatial features	✓	97.6	96.6	95.2	90.0	94.9
UniVLA [9]	spatial features	✓	96.5	96.8	95.6	92.0	95.2
Unified-VLA [51]	future visual states	✓	95.4	<b>98.8</b>	93.6	94.0	95.5
<b>OASIS (Ours)</b>	SE(3)-supervised features	×	<b>99.0</b>	<b>98.8</b>	<b>97.4</b>	<b>95.2</b>	<b>97.6</b>

Table 2: Comparison of different methods on the CALVIN ABC→D benchmark. The Pretrain column indicates whether the policy is pre-trained on large-scale robotic datasets. Tasks completed in a row measures the success rate in percent of sequentially executing 1 to 5 instructions without scene resets. Avg. denotes the average number of successful tasks per episode. † uses multi-view RGB-D.

Method	Intermediate	Pretrain	Tasks Completed in a Row					Avg.
			1	2	3	4	5	
SuSIE [4]	future visual states	✓	87.0	69.0	49.0	38.0	26.0	2.69
3D Diffuser Actor† [21]	3D feature	×	93.8	80.3	66.2	53.3	41.2	3.35
ReconVLA [45]	spatial features	✓	95.6	87.6	76.9	69.3	64.1	3.95
Seer-Large [48]	future visual states	✓	96.3	91.6	86.1	80.3	74.0	4.28
VPP [17]	future visual states	✓	96.5	90.9	86.6	82.0	76.9	4.33
Unified-VLA [51]	future visual states	✓	<b>98.9</b>	94.8	89.0	82.8	75.1	4.41
DreamVLA [60]	future visual states	✓	98.2	94.6	89.5	83.4	78.1	4.44
<b>OASIS (Ours)</b>	SE(3)-supervised features	×	98.1	<b>94.9</b>	<b>91.7</b>	<b>88.9</b>	<b>83.3</b>	<b>4.57</b>

Goal, and Long, each containing 10 tasks, and we evaluate every task over 50 episodes. For CALVIN, we use the challenging ABC→D setting to test OOD generalization to an unseen environment D after training on environments A, B, and C, reporting the average sequence length over 1,000 distinct instruction chains. Detailed descriptions of the simulation environments appear in Appendix B.1.

**Evaluation protocol.** The evaluation protocol for LIBERO and CALVIN uses only RGB images, language, and robot state as input. We follow this protocol, train OASIS for 50k steps per suite, and average across three seeds. Baseline numbers come from the original papers. We primarily compare against baselines that adhere to the same RGB-only input modality, and include 3D Diffuser Actor [21] as a structured-pose policy in Table 2, although it consumes calibrated multi-view RGB-D.

**LIBERO simulation results.** As reported in Table 1, OASIS reaches a 97.6% average success rate on LIBERO, leading the next-best baseline Unified-VLA [51] by 2.1%. The lead is consistent across all four suites, with margins of 1.4% on Spatial, 1.6% on Goal, and 1.2% on Long over the strongest prior result on each suite, and a tie on Object. As a baseline under the same protocol, ThinkAct [18] predicts a 2D image-plane trajectory while OASIS predicts an  $SE(3)$  trajectory in the camera frame, and OASIS leads ThinkAct by 13.2% on average and 24.3% on Long.

**CALVIN simulation results.** As reported in Table 2, OASIS attains an average sequence length of 4.57 on CALVIN ABC→D, ahead of every baseline. The gap widens on the five-consecutive-task setting, where OASIS reaches 83.3% and leads the next-best baseline DreamVLA [60] by 5.2%. This widening lead suggests that small per-step errors accumulate less under an intermediate aligned via  $SE(3)$  trajectory prediction than under intermediates that live in the observation space.

**Visualization of the  $SE(3)$  trajectory.** To validate the trajectory predictor qualitatively, we plot in Figure 3 the predicted translation waypoints and rotation axes alongside the executed end-effector path on four complex tasks. The execution closely tracks both the predicted positions and orientations, evidence that the predictor produces consistent rigid-body motion priors for action generation.

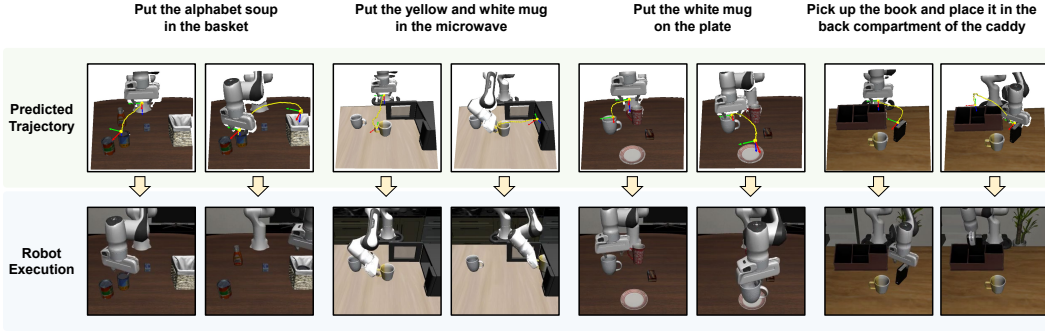


Figure 3: Visualization of the  $SE(3)$  trajectory prediction and robot execution.

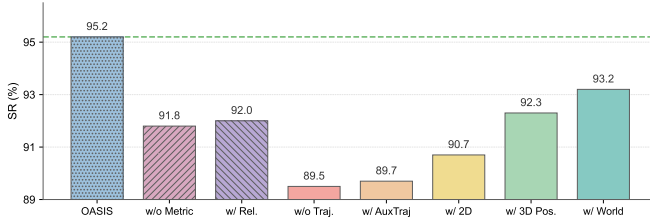


Figure 4: Ablation summary on LIBERO-Long.

Table 3: Ablation on choices of  $SO(3)$  parameterization.

Method	SR (%)
Axis-Angle	<b>95.2</b>
Quaternion	91.6
Euler Angles	92.2

### 5.3 Ablation Study

To answer questions two and three, we ablate the metric depth, the  $SE(3)$  trajectory predictor, and the  $SO(3)$  parameterization on LIBERO-Long. The same ablations are repeated on LIBERO-Spatial in Appendix B.2, where the ranking among variants is consistent.

**Effectiveness of the 3D-aware feature encoder.** The two hatched bars adjacent to the OASIS bar in Figure 4 ablate the metric depth feature. The variant *w/o Metric* drops LIBERO-Long from 95.2% to 91.8%, and the variant *w/ Rel.*, which substitutes the relative depth of Depth Anything 2, recovers only marginally to 92.0%. Metric scale, not depth in general, is what helps the 3D-aware representation.

**Impact of  $SE(3)$  trajectory prediction.** Figure 4 sweeps the supervision target on the pose-supervised hidden states under a matched-backbone control, with all variants sharing the encoder, depth model, architecture, and training budget. Richer geometric targets yield a monotonic increase on LIBERO-Long from 89.5% to 95.2%. The variant *w/o Traj.* drops the trajectory predictor and reaches 89.5%, marking the floor of the ladder. *w/ AuxTraj* retains the trajectory loss but routes it through a parallel predictor branch, so only  $\mathbf{h}_t^{3D}$ , not  $\mathbf{h}_{\text{traj}}$ , conditions the decoder. It climbs only to 89.7%, showing that pose supervision helps only when the supervised hidden states reach the decoder. *w/ 2D* reaches 90.7%, barely above *w/o Traj.*, since image-plane geometry lacks the rigid-body structure of the action space. Adding depth lifts *w/ 3D Pos.* to 92.3%, and adding rotation lifts *w/ World* to 93.2%, 2.0 points below the camera-frame counterpart. Camera-frame  $SE(3)$  attains the highest, consistent with camera-frame prediction sparing the predictor from recovering the camera-to-world extrinsic. Appendix B.3 further shows that replacing the learned decoder with a hardcoded pipeline collapses LIBERO-Spatial to 12.4% and LIBERO-Long to 0.0%, confirming the decoder is necessary to absorb extrinsic-calibration residuals, prediction noise, and gripper timing.

**Choice of  $SO(3)$  parameterization.** Table 3 compares three  $SO(3)$  parameterizations. Axis-angle reaches 95.2%, while Euler angles reach 92.2% and quaternions reach 91.6%. This ranking is consistent with axis-angle being a minimal, constraint-free chart that covers the bounded range of camera-frame end-effector orientations encountered in tabletop manipulation.

### 5.4 Real-world Experiments

**Real-world setup.** To answer the fourth question, we evaluate OASIS on a Franka Research 3 and a Kinova Gen3, shown in Figure 5. Three suites probe instruction following, spatial reasoning, and long-horizon manipulation, denoted Goal, Spatial, and Long. OASIS and the compared baselines are

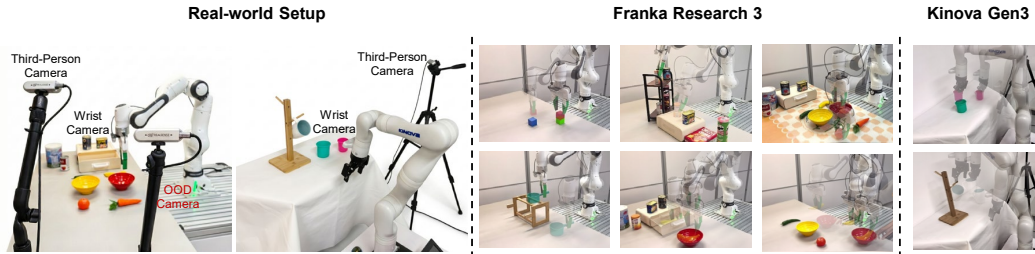


Figure 5: Real-world robot platform and task examples.

Table 4: Success rates on multi-task, spatial, and long-horizon real-world experimental settings.

Method	Goal	Spatial	Long	Average
ACT [63]	58.3	45.0	18.3	40.5
Seer-Large [48]	73.3	55.2	46.7	58.4
RDT [35]	81.7	66.7	60.0	69.5
$\pi_{0.5}$ [5]	95.0	78.3	71.6	81.6
<b>OASIS (Ours)</b>	<b>98.6</b>	<b>85.8</b>	<b>83.3</b>	<b>89.2</b>

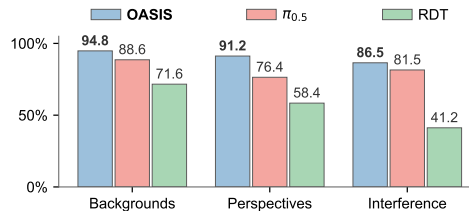


Figure 6: Success rates on Goal tasks across three OOD real-world settings.

fine-tuned on 50 teleoperated demonstrations per task and evaluated over three independent runs of 20 trials each, for 60 trials per task, exceeding the trial counts reported in the original baseline papers. OOD perturbations are further tested on the Goal task under unseen backgrounds, an altered camera viewpoint, and human interference. Full settings and task descriptions appear in Appendix C.1.

**Main results analysis.** As reported in Table 4, OASIS reaches an 89.2% average success rate, including 98.6% on Goal, 85.8% on Spatial, and 83.3% on Long, leading  $\pi_{0.5}$  [5] by 7.6%, RDT [35] by 19.7%, Seer-Large [48] by 30.8%, and ACT [63] by 48.7%, with the lead holding across all three suites. A data-scaling study in Appendix C.2 shows that on the real-world Long task, OASIS matches the 25-demonstration success rate of  $\pi_{0.5}$  with only 10 demonstrations, a low-data advantage on this task. A failure analysis in the same appendix traces OASIS’s residual errors to millimeter-scale placement and to compounding across long-horizon stages.

**OOD results analysis.** As shown in Figure 6, OASIS holds 94.8%, 91.2%, and 86.5% across unseen backgrounds, altered camera, and human interference, while  $\pi_{0.5}$  reaches 88.6%, 76.4%, and 81.5%. Under unseen backgrounds, the metric-depth feature keys off scene geometry, so distractor objects and tabletops barely shift the decoder input. Under the altered camera, only the third-person view is displaced, and because  $\mathbf{h}_t^{3D}$  and  $\mathcal{T}_t^c$  both live in the camera frame, the decoder tolerates this displacement somewhat. Under human interference, the predictor regenerates the trajectory at each step, so OASIS retargets within one action chunk when the bowl is moved mid-execution. The residual robustness of  $\pi_{0.5}$  and RDT likely reflects their large-scale robotic pretraining.

## 6 Conclusion

Existing visuomotor policies decode 6-DoF actions from intermediate representations that do not share the rigid-body geometry of the action space. We address this gap by aligning the intermediate representation with the action space via camera-frame  $SE(3)$  end-effector trajectory prediction, instantiated as OASIS, whose action decoder cross-attends to the predictor’s pose-supervised hidden states. Across simulation benchmarks and real-world platforms, OASIS attains superior manipulation precision and generalization, suggesting that aligning the intermediate is a more direct lever for visuomotor policy performance.

**Limitations and future work.** Our current method focuses on tabletop manipulation with a single robotic arm, so the  $SE(3)$  intermediate aligns with the action space of a single end-effector. Extending this design principle to richer action spaces is a natural next step, including coupled  $SE(2) \times SE(3)$  trajectories for mobile manipulation and contact-conditioned trajectories for dexterous hands.

## References

- [1] Shuai Bai, Keqin Chen, Xuejing Liu, Jialin Wang, Wenbin Ge, Sibao Song, Kai Dang, Peng Wang, Shijie Wang, Jun Tang, et al. Qwen2. 5-vl technical report. *arXiv preprint arXiv:2502.13923*, 2025.
- [2] Lucas Beyer, Andreas Steiner, André Susano Pinto, Alexander Kolesnikov, Xiao Wang, Daniel Salz, Maxim Neumann, Ibrahim Alabdulmohsin, Michael Tschannen, Emanuele Bugliarello, et al. Paligemma: A versatile 3b vlm for transfer. *arXiv preprint arXiv:2407.07726*, 2024.
- [3] Johan Bjorck, Fernando Castañeda, Nikita Cherniadev, Xingye Da, Runyu Ding, Linxi Fan, Yu Fang, Dieter Fox, Fengyuan Hu, Spencer Huang, et al. Gr00t n1: An open foundation model for generalist humanoid robots. *arXiv preprint arXiv:2503.14734*, 2025.
- [4] Kevin Black, Mitsuhiko Nakamoto, Pranav Atreya, Homer Walke, Chelsea Finn, Aviral Kumar, and Sergey Levine. Zero-shot robotic manipulation with pretrained image-editing diffusion models. *arXiv preprint arXiv:2310.10639*, 2023.
- [5] Kevin Black, Noah Brown, James Darpinian, Karan Dhabalia, Danny Driess, Adnan Esmail, Michael Robert Equi, Chelsea Finn, Niccolo Fusai, Manuel Y. Galliker, Dibya Ghosh, Lachy Groom, Karol Hausman, brian ichter, Szymon Jakubczak, Tim Jones, Liyiming Ke, Devin LeBlanc, Sergey Levine, Adrian Li-Bell, Mohith Mothukuri, Suraj Nair, Karl Pertsch, Allen Z. Ren, Lucy Xiaoyang Shi, Laura Smith, Jost Tobias Springenberg, Kyle Stachowicz, James Tanner, Quan Vuong, Homer Walke, Anna Walling, Haohuan Wang, Lili Yu, and Ury Zhilinsky.  $\pi_{0.5}$ : a vision-language-action model with open-world generalization. In *Proceedings of The 9th Conference on Robot Learning*, volume 305 of *Proceedings of Machine Learning Research*, pages 17–40. PMLR, 27–30 Sep 2025.
- [6] Kevin Black, Noah Brown, Danny Driess, Adnan Esmail, Michael Robert Equi, Chelsea Finn, Niccolo Fusai, Lachy Groom, Karol Hausman, Brian Ichter, Szymon Jakubczak, Tim Jones, Liyiming Ke, Sergey Levine, Adrian Li-Bell, Mohith Mothukuri, Suraj Nair, Karl Pertsch, Lucy Xiaoyang Shi, Laura Smith, James Tanner, Quan Vuong, Anna Walling, Haohuan Wang, and Ury Zhilinsky.  $\pi_0$ : A Vision-Language-Action Flow Model for General Robot Control. In *Proceedings of Robotics: Science and Systems*, LosAngeles, CA, USA, June 2025.
- [7] Anthony Brohan, Noah Brown, Justice Carbajal, Yevgen Chebotar, Joseph Dabis, Chelsea Finn, Keerthana Gopalakrishnan, Karol Hausman, Alex Herzog, Jasmine Hsu, et al. Rt-1: Robotics transformer for real-world control at scale. *arXiv preprint arXiv:2212.06817*, 2022.
- [8] Qingwen Bu, Hongyang Li, Li Chen, Jisong Cai, Jia Zeng, Heming Cui, Maoqing Yao, and Yu Qiao. Towards synergistic, generalized, and efficient dual-system for robotic manipulation. *arXiv preprint arXiv:2410.08001*, 2024.
- [9] Qingwen Bu, Yanting Yang, Jisong Cai, Shenyuan Gao, Guanghui Ren, Maoqing Yao, Ping Luo, and Hongyang Li. Learning to Act Anywhere with Task-centric Latent Actions. In *Proceedings of Robotics: Science and Systems*, LosAngeles, CA, USA, June 2025.
- [10] Jun Cen, Chaohui Yu, Hangjie Yuan, Yuming Jiang, Siteng Huang, Jiayan Guo, Xin Li, Yibing Song, Hao Luo, Fan Wang, et al. Worldvla: Towards autoregressive action world model. *arXiv preprint arXiv:2506.21539*, 2025.
- [11] Chi-Lam Cheang, Guangzeng Chen, Ya Jing, Tao Kong, Hang Li, Yifeng Li, Yuxiao Liu, Hongtao Wu, Jiafeng Xu, Yichu Yang, et al. Gr-2: A generative video-language-action model with web-scale knowledge for robot manipulation. *arXiv preprint arXiv:2410.06158*, 2024.
- [12] Cheng Chi, Zhenjia Xu, Siyuan Feng, Eric Cousineau, Yilun Du, Benjamin Burchfiel, Russ Tedrake, and Shuran Song. Diffusion policy: Visuomotor policy learning via action diffusion. *The International Journal of Robotics Research*, 44(10-11):1684–1704, 2025.
- [13] Yilun Du, Sherry Yang, Bo Dai, Hanjun Dai, Ofir Nachum, Josh Tenenbaum, Dale Schuurmans, and Pieter Abbeel. Learning universal policies via text-guided video generation. *Advances in neural information processing systems*, 36:9156–9172, 2023.

- [14] Theophile Gervet, Zhou Xian, Nikolaos Gkanatsios, and Katerina Fragkiadaki. Act3d: 3d feature field transformers for multi-task robotic manipulation. *arXiv preprint arXiv:2306.17817*, 2023.
- [15] Ankit Goyal, Valts Blukis, Jie Xu, Yijie Guo, Yu-Wei Chao, and Dieter Fox. Rvt-2: Learning precise manipulation from few demonstrations. *arXiv preprint arXiv:2406.08545*, 2024.
- [16] Edward J Hu, Yelong Shen, Phillip Wallis, Zeyuan Allen-Zhu, Yuanzhi Li, Shean Wang, Lu Wang, and Weizhu Chen. LoRA: Low-rank adaptation of large language models. In *International Conference on Learning Representations*, 2022.
- [17] Yucheng Hu, Yanjiang Guo, Pengchao Wang, Xiaoyu Chen, Yen-Jen Wang, Jianke Zhang, Koushil Sreenath, Chaochao Lu, and Jianyu Chen. Video prediction policy: A generalist robot policy with predictive visual representations. In *Forty-second International Conference on Machine Learning*, 2025.
- [18] Chi-Pin Huang, Yueh-Hua Wu, Min-Hung Chen, Yu-Chiang Frank Wang, and Fu-En Yang. Thinkact: Vision-language-action reasoning via reinforced visual latent planning. In *The Thirty-ninth Annual Conference on Neural Information Processing Systems*, 2025.
- [19] Yueru Jia, Jiaming Liu, Sixiang Chen, Chenyang Gu, Zhilue Wang, Longzan Luo, Lily Lee, Pengwei Wang, Zhongyuan Wang, Renrui Zhang, et al. Lift3d foundation policy: Lifting 2d large-scale pretrained models for robust 3d robotic manipulation. *arXiv preprint arXiv:2411.18623*, 2024.
- [20] Siddharth Karamcheti, Suraj Nair, Ashwin Balakrishna, Percy Liang, Thomas Kollar, and Dorsa Sadigh. Prismatic vlms: Investigating the design space of visually-conditioned language models. In *Forty-first International Conference on Machine Learning*, 2024.
- [21] Tsung-Wei Ke, Nikolaos Gkanatsios, and Katerina Fragkiadaki. 3d diffuser actor: Policy diffusion with 3d scene representations. *arXiv preprint arXiv:2402.10885*, 2024.
- [22] Moo Jin Kim, Karl Pertsch, Siddharth Karamcheti, Ted Xiao, Ashwin Balakrishna, Suraj Nair, Rafael Rafailov, Ethan Foster, Grace Lam, Pannag Sanketi, et al. Openvla: An open-source vision-language-action model. *arXiv preprint arXiv:2406.09246*, 2024.
- [23] Jason Lee, Jiafei Duan, Haoquan Fang, Yuquan Deng, Shuo Liu, Boyang Li, Bohan Fang, Jieyu Zhang, Yi Ru Wang, Sangho Lee, et al. Molmoact: Action reasoning models that can reason in space. *arXiv preprint arXiv:2508.07917*, 2025.
- [24] Chengmeng Li, Junjie Wen, Yan Peng, Yaxin Peng, Feifei Feng, and Yichen Zhu. Pointvla: Injecting the 3d world into vision-language-action models. *arXiv preprint arXiv:2503.07511*, 2025.
- [25] Peiyan Li, Yixiang Chen, Hongtao Wu, Xiao Ma, Xiangnan Wu, Yan Huang, Liang Wang, Tao Kong, and Tieniu Tan. BridgeVLA: Input-output alignment for efficient 3d manipulation learning with vision-language models. In *The Thirty-ninth Annual Conference on Neural Information Processing Systems*, 2025.
- [26] Xinghang Li, Peiyan Li, Minghuan Liu, Dong Wang, Jirong Liu, Bingyi Kang, Xiao Ma, Tao Kong, Hanbo Zhang, and Huaping Liu. Towards generalist robot policies: What matters in building vision-language-action models. *arXiv preprint arXiv:2412.14058*, 2024.
- [27] Xinghang Li, Minghuan Liu, Hanbo Zhang, Cunjun Yu, Jie Xu, Hongtao Wu, Chilam Cheang, Ya Jing, Weinan Zhang, Huaping Liu, Hang Li, and Tao Kong. Vision-language foundation models as effective robot imitators. In *The Twelfth International Conference on Learning Representations*, 2024.
- [28] Yixuan Li, Yuhui Chen, Mingcai Zhou, Haoran Li, Zhengtao Zhang, and Dongbin Zhao. Qdepthvla: quantized depth prediction as auxiliary supervision for vision-language-action models. *arXiv preprint arXiv:2510.14836*, 2025.

- [29] Fanqi Lin, Yingdong Hu, Pingyue Sheng, Chuan Wen, Jiacheng You, and Yang Gao. Data scaling laws in imitation learning for robotic manipulation. In *The Thirteenth International Conference on Learning Representations*, 2024.
- [30] Haotong Lin, Sili Chen, Junhao Liew, Donny Y Chen, Zhenyu Li, Guang Shi, Jiashi Feng, and Bingyi Kang. Depth anything 3: Recovering the visual space from any views. *arXiv preprint arXiv:2511.10647*, 2025.
- [31] Yaron Lipman, Ricky T. Q. Chen, Heli Ben-Hamu, Maximilian Nickel, and Matthew Le. Flow matching for generative modeling. In *The Eleventh International Conference on Learning Representations*, 2023.
- [32] Bo Liu, Yifeng Zhu, Chongkai Gao, Yihao Feng, Qiang Liu, Yuke Zhu, and Peter Stone. Libero: Benchmarking knowledge transfer for lifelong robot learning. *Advances in Neural Information Processing Systems*, 36:44776–44791, 2023.
- [33] Dongxiu Liu, Haoyi Niu, Zhihao Wang, Jinliang Zheng, Yinan Zheng, Zhonghong Ou, Jianming HU, Jianxiong Li, and Xianyuan Zhan. Efficient robotic policy learning via latent space backward planning. In *Forty-second International Conference on Machine Learning*, 2025.
- [34] Haotian Liu, Chunyuan Li, Qingyang Wu, and Yong Jae Lee. Visual instruction tuning. In *Thirty-seventh Conference on Neural Information Processing Systems*, 2023.
- [35] Songming Liu, Lingxuan Wu, Bangguo Li, Hengkai Tan, Huayu Chen, Zhengyi Wang, Ke Xu, Hang Su, and Jun Zhu. RDT-1b: a diffusion foundation model for bimanual manipulation. In *The Thirteenth International Conference on Learning Representations*, 2025.
- [36] Oier Mees, Lukas Hermann, Erick Rosete-Beas, and Wolfram Burgard. Calvin: A benchmark for language-conditioned policy learning for long-horizon robot manipulation tasks. *IEEE Robotics and Automation Letters*, 7(3):7327–7334, 2022.
- [37] Octo Model Team, Dibya Ghosh, Homer Walke, Karl Pertsch, Kevin Black, Oier Mees, Sudeep Dasari, Joey Hejna, Charles Xu, Jianlan Luo, Tobias Kreiman, You Liang Tan, Pannag Sanketi, Quan Vuong, Ted Xiao, Dorsa Sadigh, Chelsea Finn, and Sergey Levine. Octo: An open-source generalist robot policy. In *Proceedings of Robotics: Science and Systems*, Delft, Netherlands, 2024.
- [38] Maxime Oquab, Timothée Darcet, Théo Moutakanni, Huy V. Vo, Marc Szafraniec, Vasil Khalidov, Pierre Fernandez, Daniel HAZIZA, Francisco Massa, Alaaeldin El-Nouby, Mido Assran, Nicolas Ballas, Wojciech Galuba, Russell Howes, Po-Yao Huang, Shang-Wen Li, Ishan Misra, Michael Rabbat, Vasu Sharma, Gabriel Synnaeve, Hu Xu, Herve Jegou, Julien Mairal, Patrick Labatut, Armand Joulin, and Piotr Bojanowski. DINOv2: Learning robust visual features without supervision. *Transactions on Machine Learning Research*, 2024. ISSN 2835-8856.
- [39] Abby O’Neill, Abdul Rehman, Abhiram Maddukuri, Abhishek Gupta, Abhishek Padalkar, Abraham Lee, Acorn Pooley, Agrim Gupta, Ajay Mandlekar, Ajinkya Jain, et al. Open x-embodiment: Robotic learning datasets and rt-x models: Open x-embodiment collaboration 0. In *2024 IEEE International Conference on Robotics and Automation (ICRA)*, pages 6892–6903. IEEE, 2024.
- [40] Delin Qu, Haoming Song, Qizhi Chen, Yuanqi Yao, Xinyi Ye, Yan Ding, Zhigang Wang, JiaYuan Gu, Bin Zhao, Dong Wang, et al. Spatialv1a: Exploring spatial representations for visual-language-action model. *arXiv preprint arXiv:2501.15830*, 2025.
- [41] Kanchana Ranasinghe, Xiang Li, E-Ro Nguyen, Cristina Mata, Jongwoo Park, and Michael S Ryoo. Pixel motion as universal representation for robot control. *arXiv preprint arXiv:2505.07817*, 2025.
- [42] Moritz Reuss, Ömer Erdiñç Yağmurlu, Fabian Wenzel, and Rudolf Lioutikov. Multimodal Diffusion Transformer: Learning Versatile Behavior from Multimodal Goals. In *Proceedings of Robotics: Science and Systems*, Delft, Netherlands, July 2024.

- [43] Moritz Reuss, Jyothish Pari, Pulkit Agrawal, and Rudolf Lioutikov. Efficient diffusion transformer policies with mixture of expert denoisers for multitask learning. In *The Thirteenth International Conference on Learning Representations*, 2025.
- [44] Mohit Shridhar, Lucas Manuelli, and Dieter Fox. Perceiver-actor: A multi-task transformer for robotic manipulation. In *Conference on Robot Learning*, pages 785–799. PMLR, 2023.
- [45] Wenxuan Song, Ziyang Zhou, Han Zhao, Jiayi Chen, Pengxiang Ding, Haodong Yan, Yuxin Huang, Feilong Tang, Donglin Wang, and Haoang Li. Reconvla: Reconstructive vision-language-action model as effective robot perceiver. In *Proceedings of the AAAI Conference on Artificial Intelligence*, volume 40, pages 18549–18557, 2026.
- [46] Jianlin Su, Murtadha Ahmed, Yu Lu, Shengfeng Pan, Wen Bo, and Yunfeng Liu. Roformer: Enhanced transformer with rotary position embedding. *Neurocomputing*, 568:127063, 2024.
- [47] Yanchao Sun, Shuang Ma, Ratnesh Madaan, Rogerio Bonatti, Furong Huang, and Ashish Kapoor. SMART: Self-supervised multi-task pretraining with control transformers. In *International Conference on Learning Representations*, 2023.
- [48] Yang Tian, Sizhe Yang, Jia Zeng, Ping Wang, Dahua Lin, Hao Dong, and Jiangmiao Pang. Predictive inverse dynamics models are scalable learners for robotic manipulation. In *The Thirteenth International Conference on Learning Representations*, 2025.
- [49] Hugo Touvron, Louis Martin, Kevin Stone, Peter Albert, Amjad Almahairi, Yasmine Babaei, Nikolay Bashlykov, Soumya Batra, Prajjwal Bhargava, Shruti Bhosale, et al. Llama 2: Open foundation and fine-tuned chat models. *arXiv preprint arXiv:2307.09288*, 2023.
- [50] Jianyuan Wang, Minghao Chen, Nikita Karaev, Andrea Vedaldi, Christian Rupprecht, and David Novotny. Vggt: Visual geometry grounded transformer. In *Proceedings of the IEEE/CVF Conference on Computer Vision and Pattern Recognition*, 2025.
- [51] Yuqi Wang, Xinghang Li, Wenxuan Wang, Junbo Zhang, Yingyan Li, Yuntao Chen, Xinlong Wang, and Zhaoxiang Zhang. Unified vision-language-action model. *arXiv preprint arXiv:2506.19850*, 2025.
- [52] Chuan Wen, Xingyu Lin, John So, Kai Chen, Qi Dou, Yang Gao, and Pieter Abbeel. Any-point trajectory modeling for policy learning. *arXiv preprint arXiv:2401.00025*, 2023.
- [53] Amber Xie, Oleh Rybkin, Dorsa Sadigh, and Chelsea Finn. Latent diffusion planning for imitation learning. *arXiv preprint arXiv:2504.16925*, 2025.
- [54] Lihe Yang, Bingyi Kang, Zilong Huang, Zhen Zhao, Xiaogang Xu, Jiashi Feng, and Hengshuang Zhao. Depth anything v2. In *The Thirty-eighth Annual Conference on Neural Information Processing Systems*, 2024.
- [55] Yang Yue, Yulin Wang, Bingyi Kang, Yizeng Han, Shenzhi Wang, Shiji Song, Jiashi Feng, and Gao Huang. Deer-VLA: Dynamic inference of multimodal large language models for efficient robot execution. In *The Thirty-eighth Annual Conference on Neural Information Processing Systems*, 2024.
- [56] Yanjie Ze, Gu Zhang, Kangning Zhang, Chenyuan Hu, Muhan Wang, and Huazhe Xu. 3d diffusion policy: Generalizable visuomotor policy learning via simple 3d representations. In *Proceedings of Robotics: Science and Systems (RSS)*, 2024.
- [57] Xiaohua Zhai, Basil Mustafa, Alexander Kolesnikov, and Lucas Beyer. Sigmoid loss for language image pre-training. In *Proceedings of the IEEE/CVF international conference on computer vision*, pages 11975–11986, 2023.
- [58] Jianke Zhang, Yanjiang Guo, Yucheng Hu, Xiaoyu Chen, Xiang Zhu, and Jianyu Chen. UP-VLA: A unified understanding and prediction model for embodied agent. In *Forty-second International Conference on Machine Learning*, 2025.
- [59] Kaidong Zhang, Pengzhen Ren, Bingqian Lin, Junfan Lin, Shikui Ma, Hang Xu, and Xiaodan Liang. Pivot-r: Primitive-driven waypoint-aware world model for robotic manipulation. *Advances in Neural Information Processing Systems*, 37:54105–54136, 2024.

- [60] Wenyao Zhang, Hongsi Liu, Zekun Qi, Yunnan Wang, Xinqiang Yu, Jiazhao Zhang, Runpei Dong, Jiawei He, Fan Lu, He Wang, et al. Dreamvla: a vision-language-action model dreamed with comprehensive world knowledge. *arXiv preprint arXiv:2507.04447*, 2025.
- [61] Xinyu Zhang and Abdeslam Boularias. One-shot imitation learning with invariance matching for robotic manipulation. In *Proceedings of Robotics: Science and Systems*, Delft, Netherlands, 2024.
- [62] Qingqing Zhao, Yao Lu, Moo Jin Kim, Zipeng Fu, Zhuoyang Zhang, Yecheng Wu, Zhaoshuo Li, Qianli Ma, Song Han, Chelsea Finn, et al. Cot-vla: Visual chain-of-thought reasoning for vision-language-action models. In *Proceedings of the Computer Vision and Pattern Recognition Conference*, pages 1702–1713, 2025.
- [63] Tony Z Zhao, Vikash Kumar, Sergey Levine, and Chelsea Finn. Learning fine-grained bimanual manipulation with low-cost hardware. *arXiv preprint arXiv:2304.13705*, 2023.
- [64] Haoyu Zhen, Xiaowen Qiu, Peihao Chen, Jincheng Yang, Xin Yan, Yilun Du, Yining Hong, and Chuang Gan. 3d-vla: A 3d vision-language-action generative world model. *arXiv preprint arXiv:2403.09631*, 2024.
- [65] Ruijie Zheng, Yongyuan Liang, Shuaiyi Huang, Jianfeng Gao, Hal Daumé III, Andrey Kolobov, Furong Huang, and Jianwei Yang. TraceVLA: Visual trace prompting enhances spatial-temporal awareness for generalist robotic policies. In *The Thirteenth International Conference on Learning Representations*, 2025.
- [66] Chuning Zhu, Raymond Yu, Siyuan Feng, Benjamin Burchfiel, Paarth Shah, and Abhishek Gupta. Unified world models: Coupling video and action diffusion for pretraining on large robotic datasets. In *Proceedings of Robotics: Science and Systems (RSS)*, 2025.
- [67] Brianna Zitkovich, Tianhe Yu, Sichun Xu, Peng Xu, Ted Xiao, Fei Xia, Jialin Wu, Paul Wohlhart, Stefan Welker, Ayzaan Wahid, et al. Rt-2: Vision-language-action models transfer web knowledge to robotic control. In *Conference on Robot Learning*, pages 2165–2183. PMLR, 2023.

## A Implementation details

### A.1 OASIS architecture

Given the real-time constraints of visuomotor policies for robotic manipulation, we prioritize a lightweight pre-trained VLM over heavily parameterized alternatives. The trajectory predictor and action decoder together comprise only 70 million parameters, keeping training and inference efficient.

**Vision-language model.** OASIS employs a VLM architecture derived from Prismatic VLM [20], using Qwen2.5-0.5B [1] as the backbone and integrating two distinct visual encoders, DINOv2 [38] and SigLIP [57]. The VLM is pre-trained on the LLaVA-1.5-Instruct dataset [34], enabling it to extract rich visual and semantic information from image observations and language inputs.

**Metric depth module.** OASIS employs Depth Anything 3 [30], specifically the DA3METRIC-LARGE model, to supply spatial reasoning. Unlike Depth Anything V2 [54] and VGGT [50], which produce normalized relative depth maps, Depth Anything 3 estimates metric depth that reflects true physical distances, providing the absolute spatial information needed for precise manipulation.

**Trajectory predictor.** The trajectory predictor consists of a 4-layer Transformer architecture equipped with  $H = 8$  learnable trajectory query tokens. Within each block, these queries perform self-attention with Rotary Position Embeddings, followed by cross-attention in which the keys and values are derived from the 3D-aware representation  $\mathbf{h}_t^{3D}$ , comprising language, visual, and metric depth hidden states. The predictor outputs trajectory hidden states along with a predicted  $SE(3)$  trajectory obtained through linear projection.

**Action decoder.** The action decoder adopts the same architecture as the trajectory predictor but is reduced to 2 blocks. The cross-attention mechanism operates on the trajectory hidden states and the current robot state, which serve as keys and values. This design enables the decoder to generate actions conditioned on the  $SE(3)$  trajectory. Table 5 summarizes the architectural configurations and hyperparameters of the trajectory predictor and action decoder.

Table 5: Architecture and parameters of the trajectory predictor and action decoder.

Module	Trajectory Predictor	Action Decoder
Layers	4	2
Hidden Size	896	896
Attention Heads	8	8
Number of Queries ( $H$ )	8	8
Total Parameters	0.05B	0.02B

Table 6: Full parameter breakdown of OASIS.

Component	Total (B)	Trainable (B)
DA3METRIC-LARGE	0.35	0.00 (Frozen)
Qwen2.5-0.5B VLM	1.30	0.10 (LoRA)
Trajectory predictor + action decoder	0.07	0.07
Linear projections + state embedding	0.01	0.01
<b>Total</b>	<b>1.73</b>	<b>0.18</b>

### A.2 Training details

**Training dataset.** We use the RLDS standard datasets. Inputs consist of a language instruction, RGB images from third-person and wrist views resized to  $224 \times 224 \times 3$ , and 7-dimensional robot state inputs comprising the end-effector position, rotation, and gripper state. The policy is supervised using 6-dimensional actions and the gripper state. Trajectory supervision is derived from the world frame and projected into the third-person camera frame using its extrinsic matrix.

**Training settings.** We train OASIS using the AdamW optimizer. The vision-language model is fine-tuned using LoRA, the metric depth module remains frozen, and the trajectory predictor and action decoder are trained with full-parameter updates. The learning rate is set to  $2 \times 10^{-4}$  with a cosine annealing scheduler and warm-up. Table 7 summarizes the detailed training settings.

Table 7: Detailed training settings.

Setting	Value
GPUs	$4 \times$ NVIDIA A800
Global Batch Size	64 (16 per device)
Training Steps	50,000
Random Seeds	3 (results averaged)
Optimizer	AdamW
Fine-tuning Method	LoRA
Learning Rate	$2 \times 10^{-4}$
Warmup Steps	5,000

## B Additional details for simulation experiments

### B.1 Simulation benchmarks and settings

**LIBERO simulation benchmark.** We evaluate OASIS on the LIBERO benchmark, a comprehensive simulation suite comprising four distinct task suites, namely LIBERO-Spatial, LIBERO-Object, LIBERO-Goal, and LIBERO-Long. These suites are designed to assess specific capabilities, including spatial reasoning, object grounding, goal-directed behavior, and long-horizon planning. Each suite consists of 10 unique tasks, supported by 50 human-teleoperated demonstrations per task. To assess policy performance, we execute 50 evaluation rollouts for each task and report the average success rate. Figure 7 and Table 8 provide visual examples of the scenarios and language instructions for a subset of the tasks.

Table 8: Examples of language instructions for selected tasks in the LIBERO benchmark.

LIBERO	Task Instructions
Spatial	Pick up the black bowl from table center and place it on the plate.
	Pick up the black bowl on the stove and place it on the plate.
	...
Object	Pick up the alphabet soup and place it in the basket.
	Pick up the chocolate pudding and place it in the basket.
	...
Goal	Open the top drawer and put the bowl inside.
	Put the wine bottle on top of the cabinet.
	Turn on the stove.
...	
Long	Put the white mug on the left plate and put the yellow and white mug on the right plate.
	Put the black bowl in the bottom drawer of the cabinet and close it.
	Put the yellow and white mug in the microwave and close it.
...	

**CALVIN simulation benchmark.** We also evaluate OASIS on the CALVIN benchmark, a standardized simulation suite designed to assess long-horizon and language-conditioned robotic manipulation. The benchmark comprises four visually distinct environments, named Env A, B, C, and D, each simulating a Franka Emika Panda robot performing tabletop manipulation with diverse objects. Figure 8 provides an overview of the simulation environment, while Table 9 presents representative

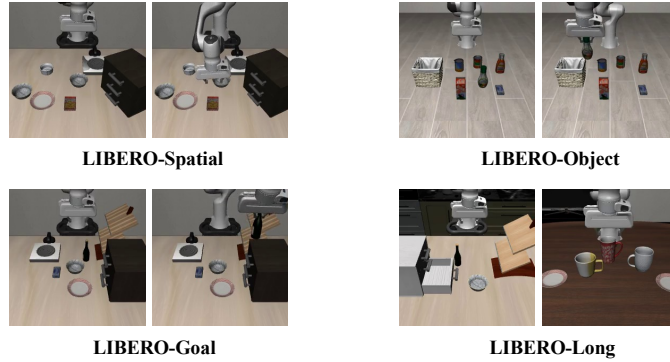


Figure 7: Example scenario from the LIBERO benchmark.

language instructions organized into eight distinct manipulation categories. Leveraging over two million human demonstration episodes, CALVIN defines 34 distinct subtasks. For evaluation, these subtasks are organized into 1,000 unique instruction chains, in which the robot must execute five consecutive commands in strict sequence. To quantify performance, we report the average sequence length and the success rate.

Table 9: Examples of language instructions for different task categories in the CALVIN benchmark.

CALVIN	Task Instructions
Turn On/Off	Turn on/off lightbulb. Turn on/off LED.
Open/Close Drawer	Open drawer. Close drawer.
Move Slider	Move slider left. Move slider right.
Rotate	Rotate red block left/right. Rotate pink block left/right. ...
Stack/Unstack	Stack block. Unstack block.
Lift	Lift red block table. Lift pink block drawer. ...
Place	Place in slider. Place in drawer.
Push	Push red block left/right. Push into drawer. ...

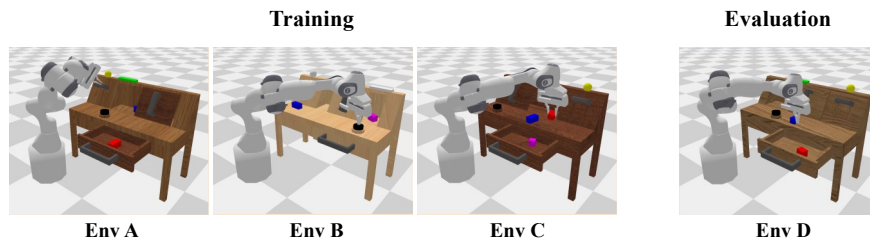


Figure 8: Example scenario from the CALVIN benchmark.

## B.2 Additional ablation results on LIBERO-Spatial

To verify that the ablation trends on LIBERO-Long generalize across task suites, we repeat the trajectory-predictor, metric-depth, and frame ablations on LIBERO-Spatial and report the success rates side by side in Table 10.

The ranking of supervision targets on LIBERO-Spatial matches that on LIBERO-Long. The monotonic ladder, from *w/o Traj.* to *w/ AuxTraj*, *w/ 2D*, *w/ 3D Pos.*, *w/ World*, and OASIS, holds on both suites, with OASIS reaching 99.0% on Spatial and 95.2% on Long. The variant *w/ 2D* matches the no-supervision baseline within seed noise on Long, at 90.7% versus 89.5%, and adds a modest gain on Spatial, at 93.3% versus 91.6%, indicating that image-plane geometry alone is too weak to align

the intermediate with the action space. Adding depth, by moving from *w/ 2D* to *w/ 3D Pos.*, adds a further 1.6 points on Long and 2.1 points on Spatial. Adding rotation, by moving from *w/ 3D Pos.* to *w/ World*, adds 0.9 and 1.1 points respectively. Camera-frame  $SE(3)$  (OASIS) beats *w/ World* by 2.0 points on Long and 2.5 points on Spatial, consistent with deferring the uncalibrated camera-to-world transform to the learned decoder as analyzed in Section 3.2.

We further note that *w/ AuxTraj* carries the trajectory predictor’s parameters while *w/o Traj.* does not. This trainable-parameter asymmetry favors *w/ AuxTraj*, so the OASIS gain of +5.5 points on LIBERO-Long and +7.1 points on LIBERO-Spatial over *w/ AuxTraj* cannot be attributed to trajectory-branch capacity, and instead reflects the contribution of routing the pose-supervised hidden states to the action decoder.

Table 10: Intermediate-type screen on LIBERO-Long and LIBERO-Spatial. All variants share the same backbone, depth model, predictor architecture, and parameter budget. Only the supervision target on the pose-supervised hidden states differs. The metric-depth ablation row is included for completeness. Both suites show a monotonic ladder in the geometric richness of the supervision target.

Variant	LIBERO-Long	LIBERO-Spatial
<i>w/o Traj.</i>	89.5	91.6
<i>w/ AuxTraj</i>	89.7	91.9
<i>w/ 2D</i>	90.7	93.3
<i>w/ 3D Pos.</i>	92.3	95.4
<i>w/ World</i>	93.2	96.5
<b>OASIS</b>	<b>95.2</b>	<b>99.0</b>
<i>w/o Metric</i>	91.8	93.4

### B.3 Closed-form decoder ablation

To probe whether the learned action decoder is reducible to closed-form geometry, we replace it with a hardcoded geometric pipeline that converts the same predicted camera-frame  $SE(3)$  trajectory into world-frame poses via known camera extrinsics and emits relative actions, with gripper open/close further supplied by privileged simulator information unavailable to OASIS. Despite this strictly stronger setting, the hardcoded pipeline collapses to 12.4% on LIBERO-Spatial and 0.0% on LIBERO-Long against OASIS’s 99.0% and 95.2% with the same trajectory predictor, as shown in Table 11. Rollouts confirm that the predicted trajectory does encode meaningful geometry, since the robot consistently moves toward the target object, but small residual prediction noise, contact dynamics, and gripper timing compound into failures that no closed-form transform can absorb. This result rules out the interpretation that OASIS reduces to a renamed closed-form execution pipeline over predicted poses, and confirms that the learned decoder is necessary.

Table 11: Closed-form decoder ablation. The hardcoded pipeline reads the same predicted  $SE(3)$  trajectory as OASIS but executes it via known camera extrinsics and privileged simulator information for the gripper, a strictly stronger setting than OASIS’s learned decoder.

Decoder	LIBERO-Spatial	LIBERO-Long
OASIS (learned decoder)	<b>99.0</b>	<b>95.2</b>
Hardcoded geometric pipeline	12.4	0.0

## C Additional details for real-world experiments

### C.1 Real-world experimental settings

To comprehensively evaluate the capabilities of OASIS, we design a diverse suite of real-world experiments categorized into three distinct tasks, namely Goal, Spatial, and Long. The language instructions used in the experiments are shown in Table 12. The complete experimental setup and the specific workflow for each task suite are visualized in Figure 9.

**Goal task.** Guided by the language instruction, the robot must place a target object into the designated container. This setup validates the semantic understanding and multitask capabilities of the visuomotor policy, demonstrating its ability to translate high-level semantic goals into precise actions. While the relative object-container position remains constant, the absolute distance from the robot base varies across trials to prevent overfitting and assess robustness to diverse initializations.



Figure 9: Real-world execution examples of Goal, Spatial, and Long tasks. The Goal task utilizes a tabletop environment with two bowls and four objects arranged in a structured layout, where the robot must place the correct object into the correct bowl based on the language instruction. The Spatial task comprises six distinct subtasks, namely stacking blocks, building towers, placing pots on wooden bracket, putting orange can on shelves, placing pink cup into cyan cup, and hanging cups on cup holders. In the Long task, the robot is required to execute a multi-stage sequence, first opening a drawer, then retrieving the banana from the drawer, and finally placing it into the red bowl.

Table 12: Examples of language instructions for real-world experiments.

Real-World Experiments	Task Instructions
Goal	Place the banana into the red bowl. Pick up the carrot and place it into the red bowl. Grasp the orange and put it into the yellow bowl. ...
Spatial	Put the pot on the wooden bracket. Stack the red cube on top of the green cube. Place the blue cube on top of the red cube. Put the orange can on the shelves. Hang the cup on the cup holder. Place the pink cup into the cyan cup.
Long	Open the drawer and place the banana into the red bowl.

**Spatial task.** These tasks require the visuomotor policy to achieve high precision in localizing and grasping objects in various poses to ensure structural stability. Specifically, the placing pots on wooden bracket task focuses on precise placement. To prevent tipping, the policy must ensure that both sides of the pot rest securely on the respective wooden bars. Moreover, the hanging cups on cup holders task requires precise placement and secure attachment. Collectively, these tasks evaluate the spatial reasoning of the policies under geometric constraints.

**Long task.** Compared to single-stage tasks, the Long task imposes stricter requirements on the visuomotor policy, demanding not only precise low-level motor control but also long-term temporal reasoning capability. Furthermore, the extended execution chain increases the risk of compounding errors, since any imprecision during the initial drawer-opening phase directly impacts the success of subsequent grasping steps. Consequently, the policy requires robust closed-loop feedback mechanisms to correct deviations in real time. This task demonstrates the robot’s potential to handle complex sequential operations.

**OOD scenario settings.** To evaluate the zero-shot generalization of OASIS, we design a suite of out-of-distribution experiments within the Goal task setting, as illustrated in Figure 10. The unseen backgrounds scenario introduces unseen objects and an unseen tabletop that were not present during training, assessing the ability of the visuomotor policies to selectively attend to task-relevant features while ignoring visual distractors. The altered camera perspectives scenario displaces only the third-person camera at test time, with translation of roughly 15 cm relative to the training viewpoint, while the wrist camera and all other components remain unchanged. No recalibration or test-time adaptation is performed for any policy. This configuration probes robustness to a single uncalibrated third-person viewpoint shift. It does not establish camera-pose invariance, which would require sweeping the full 6-DoF extrinsic space. The dynamic human interference scenario introduces perturbations in which the target bowl is relocated while the robot is transporting the object. This validates the closed-loop reactivity of the policies, examining whether they can dynamically adjust to track the moving target in real time and demonstrating their adaptability to unstructured real-world environments.

## C.2 Additional real-world experimental results

**Failure analysis.** As shown in Figure 11, OASIS’s lowest real-world success rates concentrate on subtasks that demand sub-centimeter placement or precise orientation. *Hang cup* (76.6%) fails when residual rotation errors prevent the handle from engaging the holder, and *Place pot* (83.3%) fails when small z-axis or yaw errors leave the pot resting on a single supporting bar. The *Long horizon* task (83.3%) is dominated by stage compounding: imprecision during drawer opening shifts the banana’s reachable region and propagates into grasp failures downstream.

**Inference speed analysis.** To deploy the trained policy without operating-system or code-version conflicts, we wrap model loading and inference in a WebSocket server on a remote machine. The

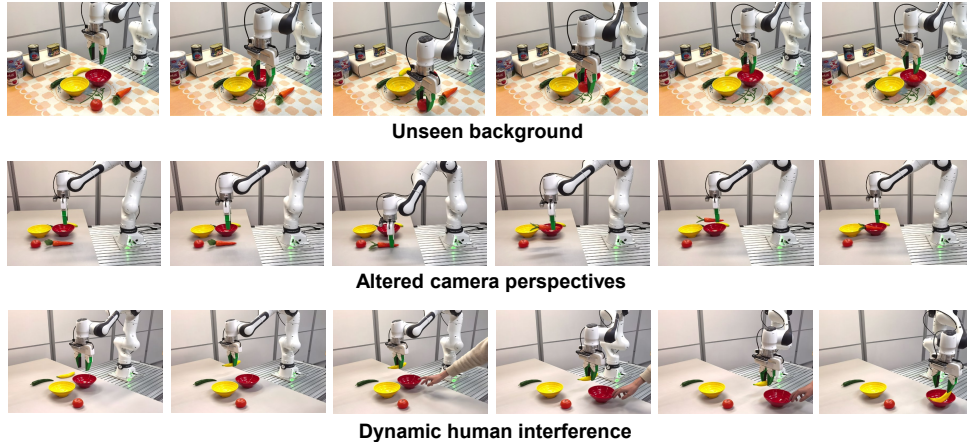


Figure 10: Real-world execution examples under OOD scenarios.

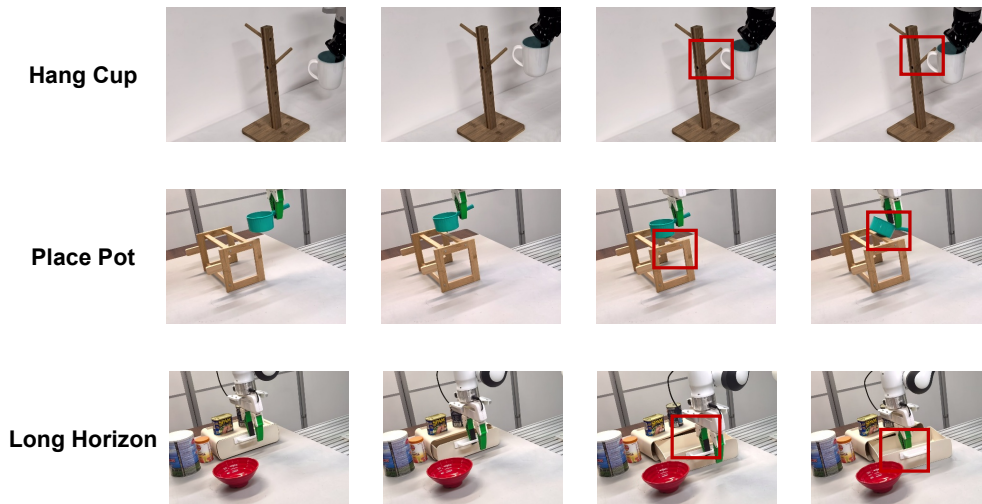


Figure 11: Failure cases of OASIS in real-world execution.

server communicates in real time with the robot’s control computer, receiving live camera images at up to 30 Hz and the end-effector state, and returning actions for execution. On an NVIDIA RTX 4090 GPU without additional computational load, the policy consumes about 4.5 GB of GPU memory. Each inference cycle predicts the  $SE(3)$  trajectory and 8 subsequent action steps, executed sequentially with a response time of about 0.05 s, corresponding to roughly 20 Hz.

**Data-scaling on the real-world Long task.** To probe how data efficiency interacts with the aligned-intermediate design, we train OASIS and  $\pi_{0.5}$  on the real-world Long task with progressively reduced demonstration budgets and evaluate each variant over three independent runs of 20 trials each, for 60 trials per configuration. Table 14 reports success rate as a function of demonstration count. With only 10 demonstrations, OASIS reaches 35.0% while  $\pi_{0.5}$  reaches 15.0%. At 25 demonstrations, OASIS reaches 55.0% while  $\pi_{0.5}$  reaches 35.0%, and at the full 50 demonstrations, OASIS reaches 83.3% while  $\pi_{0.5}$  reaches 71.6%. OASIS thus matches the observed 25-demonstration success rate of  $\pi_{0.5}$  using only 10 demonstrations on this task. We report this as a low-data advantage on this Long task rather than a universal scaling factor, since the +20 point absolute lead at 10 and 25 demonstrations narrows to +11.7 points at 50 demonstrations and is observed only on a single real-world task.

Table 13: Performance of OASIS on the Goal, Spatial, and Long tasks.

Category	Task Description	Success Rate (%)
Goal	Place the banana into the red bowl	100.0
	Place the banana into the yellow bowl	100.0
	Place the carrot into the red bowl	100.0
	Place the carrot into the yellow bowl	100.0
	Place the orange into the red bowl	95.0
	Place the orange into the yellow bowl	96.7
Spatial	Stack blocks	90.0
	Build towers	90.0
	Place pots on wooden bracket	83.3
	Put orange can on shelves	81.6
	Hang the cup	76.6
	Place the pink cup	93.3
Long	Open the drawer and place the banana into the red bowl	83.3

Table 14: Data-scaling results on the real-world Long task. We train OASIS and  $\pi_{0.5}$  with 10, 25, and the full 50 demonstrations and evaluate each variant over three independent runs of 20 trials each, for 60 trials per configuration. All numbers are success rates in percent.

Method	10 demos	25 demos	50 demos
$\pi_{0.5}$	15.0	35.0	71.6
<b>OASIS (Ours)</b>	<b>35.0</b>	<b>55.0</b>	<b>83.3</b>

### C.3 Wilson 95% confidence intervals for real-world results

To quantify finite-trial uncertainty, we report Wilson score 95% confidence intervals for the head-to-head OASIS vs  $\pi_{0.5}$  comparison on the real-world main results in Table 4. Goal and Spatial each comprise six sub-tasks evaluated over 60 trials per sub-task, so we report a pooled descriptive Wilson interval over  $n=360$  trials per suite, while Long is a single task with  $n=60$ .

Table 15: Wilson 95% confidence intervals, in percent, for OASIS vs  $\pi_{0.5}$  on the real-world main results.

Method	Goal	Spatial	Long
$\pi_{0.5}$	95.0 [92.4, 96.9]	78.3 [73.7, 82.3]	71.6 [58.9, 81.6]
<b>OASIS (Ours)</b>	<b>98.6 [96.6, 99.5]</b>	<b>85.8 [81.8, 88.9]</b>	<b>83.3 [71.7, 90.7]</b>

The Goal and Spatial intervals indicate clear separation between OASIS and  $\pi_{0.5}$ , while the Long intervals overlap. We therefore describe the Long-task gap in the main text as a numerical lead rather than a statistically significant difference.

## D Broader impacts

OASIS proposes a new design principle for visuomotor policies, aligning the intermediate representation with the action space via  $SE(3)$  end-effector trajectory prediction. Instead of decoding actions from observation-space features alone, our framework first predicts a camera-frame  $SE(3)$  trajectory whose pose-supervised hidden states condition the action decoder. This aligned intermediate improves manipulation precision and generalization across simulation benchmarks and real-world platforms.

A key strength of OASIS lies in its training efficiency and accessibility. It requires neither large-scale robotic pretraining nor annotated spatial labels, with supervision derived solely from standard

expert demonstrations. With only 0.18B trainable parameters trained on four GPUs, the framework lowers the cost barrier for research groups and small organizations developing manipulation policies on commodity hardware. The explicit separation of geometric reasoning from action execution further makes the intermediate representation inspectable, supporting transparent debugging and safer deployment than monolithic image-to-action models.

Practically, this design can benefit assistive household robots, dexterous industrial manipulators, and tabletop laboratory automation, where precise  $SE(3)$  control under modest data budgets is essential. Overall, OASIS offers a practical, training-efficient framework for improving visuomotor policies, and we hope it inspires further research into geometrically aligned intermediate representations and low-cost robot learning.